J Ther Eng, Vol. 11, No. 6, pp. 1781−1797, November, 2025

Journal of Thermal Engineering
Web page info: https://jten.yildiz.edu.tr
DOI: 10.14744/thermal.0001045

Research Article

Numerical analysis of thermo-hydraulic performance of molten salt coolant flowing through a louvered-fin compact heat exchanger

Bahadır DOĞAN[1,*], Mehmet Mete OZTURK[2,], Latife Berrin ERBAY[1]**

[1]*Department of Mechanical Engineering, Faculty of Engineering and Architecture, Eskişehir Osmangazi University, Eskişehir, 26480, Türkiye*
[2]*Transportation Vocational School, Eskişehir Technical University, Eskişehir, 26140, Türkiye*

ARTICLE INFO

Article history
Received: 23 October 2024
Revised: 15 March 2025
Accepted: 17 March 2025

Keywords:
Compact Heat Exchanger; FLiBe; Louvered Fin; Molten Salt

ABSTRACT

New types of nuclear reactors have been proposed in recent years to meet the growing energy demand. These reactors operate at high outlet temperatures, which must be efficiently removed from the system. For this purpose, compact heat exchangers are considered important candidates. The study examines the thermohydraulic behavior of LiF-BeF_2 (FLiBe) molten salt in a compact heat exchanger with multi-louvered fins as a part of a Molten Salt Reactor's cooling loop at the steady state. This numerical benchmark study aimed to collect data for both baseline scenarios and cases of slow coolant circulation within the reactor for the first time in the literature. Numerical tests were conducted for low Reynolds numbers ranging from 100 to 500, over a flow region characterized by varying fin pitches and louver angles to compare FLiBe's performance as a coolant in a Molten Salt Reactor. The findings indicate that as the louver angle increases, the molten salt flow becomes more directed through the louvers, enhancing heat transfer between the fins and the molten salt. Conversely, increasing fin pitches directs the flow more towards the ducts, reducing interaction with the FLiBe and diminishing thermal performance. As regard to outcomes, the highest heat transfer coefficient is determined to be about 27 kW/(m^2K) at the smallest fin pitch of 1.5 mm, the biggest louver angle of 36° and a molten salt inlet velocity of 0.8 m/s. Under the same conditions, the heat transfer coefficient is calculated as 24.7 kW/(m^2K) and 24.2 kW/(m^2K) for the pitches of 2.0 mm and 2.5 mm, respectively. The louver angle has a significant effect on the pressure drop especially for the fin pitch of 1.50 mm. At 0.8 m/s molten salt inlet velocity and fin pitch of 1.5 mm, the pressure drop with a louver angle of 36° is 58% higher than with a louver angle of 20°.

Cite this article as: Doğan B, Ozturk MM, Erbay LB. Numerical analysis of thermo-hydraulic performance of molten salt coolant flowing through a louvered-fin compact heat exchanger. J Ther Eng 2025;11(6):1781−1797.

***Corresponding author.**
*E-mail address: bdogan@ogu.edu.tr

**Current Affilitiaon: Department of Aeronautical Engineering, Faculty of Engineering and Architecture, Eskisehir Osmangazi University, Batı-Meşelik 26480, Eskişehir, Türkiye

This paper was recommended for publication in revised form by Editor-in-Chief Ahmet Selim Dalkilic

INTRODUCTION

In light of nuclear mishaps, public dissent, and the critical issue of climate change due to hazardous carbon emissions, the Next Generation Nuclear Plant (NGNP) initiative and the Fourth Generation Nuclear Reactor Systems (Gen IV) have identified Molten Salt Reactors (MSRs) as one of six promising candidates for reliable and sustainable nuclear power generation with minimal carbon emissions in the future. Molten salt nuclear reactors have been a subject of interest in nuclear engineering since 1940s, beginning with initial studies in Tennessee [1]. MSRs have been applied in various fields, including Aircraft Nuclear Propulsion (ANP), with successful experiments such as the aircraft reactor experiment (ARE) and aircraft reactor test (ART). Building on research from Oak Ridge National Laboratory (ORNL), small MSRs, known as Fuji, were developed by Furukawa et al. [2-5] within the Thorium Molten Salt Nuclear Energy Synergetic (THORIMS-NES) system. FLiBe, a fluid that serves both as fuel carrier and coolant, is considered one of the most suitable for use in Fuji-MSRs, facilitating heat exchange between the reactor core and the steam turbine side. Recent studies by emerging MSR firms have presented various MSR designs, yet they often lack detailed information on heat exchangers. Designing heat exchangers for MSRs poses significant challenges. Historically, ORNL has conducted extensive research on MSR heat exchanger design, particularly focusing on shell-and-tube types, and has established key design considerations well-documented in the literature [6-9]. These designs were shaped by the prevailing technology and standards applicable to shell-and-tube heat exchangers. In a novel approach, Erbay [10] explored the integration of MSRs with a Stirling heat engine, highlighting the critical need for high-performance heat exchangers to function as the hot-end head of the Stirling engine, with molten salt FLiBe flowing over and helium within the channels. In another original approach, Akram et al. [11] investigated a solar-assisted trigeneration system with molten salts from exergy aspect. Erbay's expertise [12] also shed light on the heat removal system of Fuji-MSRs [3]. Although new heat exchanger designs have been proposed in projects such as EVOL and SAMOFAR [13-15], these designs are yet to be finalized and manufactured.

Liquid coolants exhibit superior performance in gas cooling systems by minimizing temperature gradients across heat exchangers and reducing pumping power. Molten salts serve as both fuel and coolant in MSRs, chosen for their thermal efficiency and exceptional properties [16-18]. These coolants maintain chemical and radiological stability at elevated temperatures, exhibit low vapor pressures, and possess high boiling points, specific heat, and thermal conductivity. Their compatibility with high-temperature materials and cost-effectiveness further enhances their appeal. Notably, the volumetric heat capacity of molten salt coolants is nearly 25% greater than that of pressurized water and about five times that of liquid sodium, facilitating the design of compact heat exchangers due to their high heat capacity and safe operational pressures. However, molten salt experiments present several challenges. The high melting point, while beneficial, complicates convection heat transfer experiments as it requires heating the entire system, including the cooling equipment. Additionally, corrosion of pipes adds further complexity. Consequently, computational fluid dynamics (CFD) studies have become a vital tool for assessing the thermal-hydraulic properties of molten salts. Recent experimental [19-23] and numerical [1, 24-28] research has focused on elucidating the convective heat transfer characteristics of molten salts and verifying the accuracy of established empirical correlations.

To address the individual challenges of both numerical and experimental investigations on this unique topic, researchers study shell-and-tube heat exchangers for molten salt refrigerants using a comparative approach, either numerically or experimentally [29, 30]. These studies have examined various molten salts, including $LiNO_3$, LiF-NaF-KF (FLiNaK), $NaNO_2$-KNO_3-$NaNO_3$, LiF-BeF_2-ThF_4-UF_4, $NaBF_4$-NaF, and LiF-BeF_2 (FLiBe). The convective heat transfer with molten salt in different types of channel geometries; namely circular tubes, annular ducts, outside the tube bundles, and double pipes were conducted in these useful studies. The heat transfer enhancement in MSRs is important for reducing cost and fluid inventory. The amount of fuel out of the core in the MSRs should be adjusted to prevent a new critical mass. The enhancement of heat transfer and the need for a small volume to avoid hold-up issues in MSRs make compact heat exchanger configurations suitable. The Printed Circuit Heat Exchanger (PCHE), a novel design, offers compactness, low-pressure drop, high effectiveness, and the capacity to handle significant pressure differentials, and is produced by Heatric. [31, 32]. A compact heat exchanger (CHE) featuring finned surfaces tailored for a suitable working fluid is poised to become crucial in Molten Salt Reactors (MSRs). Various molten salts have undergone thorough analysis by Oak Ridge National Laboratory (ORNL) to aid the MSR Experiment and the Molten Salt Breeder Reactor Programs. [31]. Due to its convenience for both MSRs fuel salt and coolant, FLiBe has been reported as a promising candidate during the fluid selection process. Therefore, the thermal and hydraulic characteristics of FLiBe flowing over the finned surface must be investigated. Regretfully, there isn't any work that reports neither experimental nor numerical findings for a louvered fin flat-tube compact heat exchanger associated with MSRs in open sources. Computational Fluid Dynamics (CFD) can be used to fulfill the lack of data and information in the field.

This research examines a louvered fin flat-tube compact heat exchanger designed to achieve high heat transfer rates and extensive heat transfer areas. FLiBe (LiF-BeF_2), commonly used in MSRs and Molten Salt Fast Reactors (MSFRs), serve as the working fluid. The study focuses on the

steady-state thermo-hydraulic performance of FLiBe in the cooling loop of an MSR, particularly within a low-velocity range, which could represent either a primary or secondary heat exchanger. Numerical simulations were performed at low Reynolds numbers ranging from 100 to 500 to emulate scenarios like coolant pump failures. Various louver pitches and fin pitches and fin louver angles were tested. The resulting velocity profiles, temperature, and pressure fields were analyzed. Performance metrics for FLiBe as a coolant were quantified using the heat transfer coefficient, pressure drop data, Colburn *j*-factor, fanning friction factor, and the volume goodness factor. Despite concerns regarding the use of molten salts in nuclear reactors, this study aims to enrich the MSR literature by exploring alternative heat exchanger configurations. The paper begins by detailing the geometry of the louvered finned flow channel, followed by a description of the Computational Fluid Dynamics (CFD) model used to simulate FLiBe convection, and concludes with the presentation of validated results.

MATERIALS AND METHODS

The technical drawing of the louvered fin geometry under consideration is depicted in Fig. 1. The material used for the fin is Hastelloy-N, a nickel-based alloy developed by ORNL and the International Nickel Company for use in MSRs. The louvered fin's performance was evaluated for fin pitches of 1.5, 2.0, and 2.5 mm and louver angles of 20°, 24°, 28°, 32°, and 36°, while keeping the louver pitch and fin thickness constant at 1.7 mm and 0.1 mm, respectively.

As previously discussed, this study numerically investigates a compact heat exchanger featuring a louvered fin on a flat tube with FLiBe as the working fluid, to provide initial results on its suitability for use in MSRs. While a variety of working fluids are applicable for MSRs, FLiBe was selected for this research. The criteria for choosing materials are detailed in the first part of this section, followed by an explanation of the mathematical methodology in the second part.

Considerations for Coolant Selection

To improve the efficiency of the reactors, several types of working fluids have been proposed and used by researchers. Since a variety of molten salts can be used in the reactors, the selection of the right working fluid is crucial. To ease the selection, a series of the figure of merits (FOM) has been suggested by Kim et al. [33] as regards to the general characteristics that are required in the coolant (Table 1). By considering the suggested FOMs for each general characteristic of the coolants, molten salts considered in MSRs could be compared from a better aspect. The physical properties of typical molten salts used in the reactors and FOM's are summarized in Table 2. The original table could be addressed in ref. [33] in which results of not only the molten salts but also gas and liquid metals could be found as well. In Table 2, in addition to the typical molten salts reported by Kim et al. [33], the physical properties and FOM's of the FLiBe is also enlisted at the bottom in the present study.

The first one, FOM_{ht}, among the suggested FOMs, is regarding the heat transfer performance of the coolant.

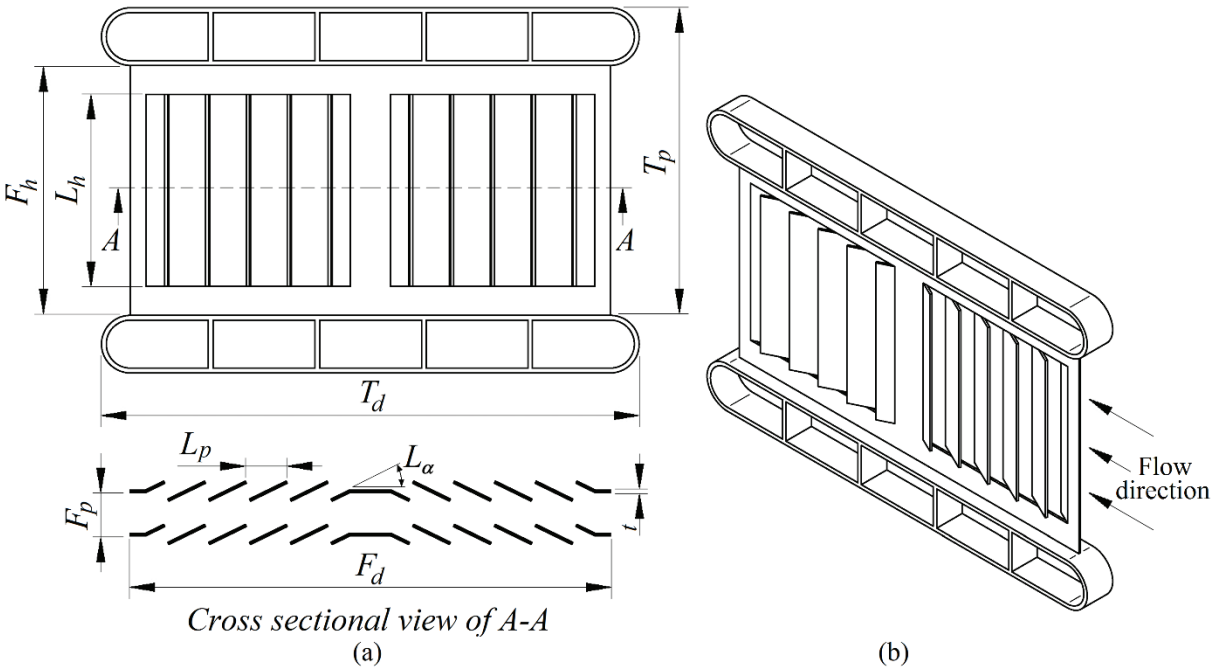

Figure 1. Technical drawing of the considered louvered fin (a) 2-D cross-sectional view of *A-A* (b) 3-D appearance.

Table 1. Definition of the figure of merits (FOMs)

Definition	FOM	
Heat transfer performance of coolant where, $FOM_{ht,0} = (k)^{0.6}\,(\rho)^{0.58}\,(C_p)^{0.4}\,(\mu)^{-0.47}$	$FOM_{ht} = \frac{(k)^{0.6}(\rho)^{0.58}\left(C_p\right)^{0.4}(\mu)^{-0.47}}{FOM_{ht,0}}$	(1)
Pumping power of coolant where $FOM_{p,0} = (\rho)^{-2}\,(C_p)^{-2.8}\,(\mu)^{02}$	$FOM_{p} = \frac{(\rho)^{-2}\left(C_p\right)^{-2.8}(\mu)^{02}}{FOM_{p,0}}$	(2)
Volume of coolant where $FOM_{cv,0} = (\rho)^{-0.84}\,(C_p)^{-1.16}\,(\mu)^{0.1}$	$FOM_{cv} = \frac{(\rho)^{-0.84}\left(C_p\right)^{-1.16}(\mu)^{0.1}}{FOM_{cv,0}}$	(3)
Volume of structural materials where $FOM_{ccv,0} = (P)\,(\rho)^{-0.84}\,(C_p)^{-1.16}\,(\mu)^{0.1}$	$FOM_{ccv} = \frac{(P)\,(\rho)^{-0.84}\left(C_p\right)^{-1.16}(\mu)^{0.1}}{FOM_{ccv,0}}$	(4)
Heat loss of the coolant where $FOM_{hl,0} = (k)^{0.6}\,(\rho)^{0.34}\,(C_p)^{0.06}\,(\mu)^{-0.44}$	$FOM_{hl} = \frac{(k)^{0.6}(\rho)^{0.34}\left(C_p\right)^{0.06}(\mu)^{-0.44}}{FOM_{hl,0}}$	(5)

Table 2. Comparison of FOMs for different coolants

Coolant	Melting Point (°C)	k	ρ	C_p	μ	P	FOM_{th}	FOM_p	FOM_{cv}	FOM_{ccv}	FOM_{hl}
		(W/mK)	(kg/m³)	(J/kgK)	(Pa·s)	(atm)	-	-	-	-	-
Water (25°C)	0	0.61	997	4181	0.00089	1	1.00	1.00	1.00	1.00	1.00
LiF-NaF-KF	454	0.92	2020	1886	0.00290	1	0.80	2.87	1.57	1.57	0.92
NaF-ZrF_4	500	0.49	3140	1173	0.00510	1	0.45	5.02	1.98	1.98	0.56
KF-ZrF_4	390	0.45	2800	1046	0.00510	1	0.38	8.70	2.50	2.50	0.51
LiF-NaF-ZrF_4	436	0.53	2920	1233	0.00690	1	0.40	5.36	2.05	2.05	0.50
LiCl-KCl	355	0.42	1520	1198	0.00115	1	0.55	14.99	3.07	3.07	0.76
LiCl-RbCl	313	0.36	1880	890	0.00130	1	0.47	23.08	3.67	3.67	0.70
NaCl-$MgCl_2$	445	0.50	1680	1096	0.00136	1	0.58	16.28	3.18	3.18	0.81
KCl-$MgCl_2$	426	0.40	1660	1160	0.00140	1	0.50	14.31	3.02	3.02	0.70
NaF-$NaBF_4$	385	0.40	1750	1507	0.00090	1	0.71	5.66	2.04	2.04	0.88
KF-KBF_4	460	0.38	1700	1305	0.00090	1	0.64	8.98	2.47	2.47	0.84
RbF-RbF_4	442	0.28	2210	909	0.00090	1	0.54	14.63	3.01	3.01	0.75
FLiBe LiF – BeF_2	459	1.00	1940	2414	0.00560	1	0.67	1.78	1.30	1.30	0.73

As for the evaluation of the findings of suggested FOM's, Kim et al. [33] reported that FOM_{ht} would get higher values while the remaining ones (FOM_p, FOM_{cv}, FOM_{ccv} and FOM_{hl}) would get lower values to achieve a better performance. From the highlighted point of view, it is seen that FLiBe is superior than the alternative molten salts. Though it has moderate FOM_{ht}, it has the lowest FOM's in remaining four FOMs.

Numerical Method

Considering that the maximum velocity in each section of the heat exchanger must be limited to 5 m/s to prevent erosion and corrosion [14], the FLiBe flow was presumed to be laminar for $Re_{Lp} \leq 1300$ [34]. The mass, momentum, and energy equations for two-dimensional, steady, laminar, and incompressible flow are provided respectively in Eqs. 6-8.

$$\nabla \cdot V = 0 \tag{6}$$

$$(V \cdot \nabla)V = -\frac{1}{\rho}\nabla P + \upsilon \nabla^2 V \tag{7}$$

$$(V \cdot \nabla)T = \alpha \nabla^2 T \tag{8}$$

In modeling and analysis of the primary and secondary heat exchangers with louvered fins in MSRs, the expected properties of FLiBe and Hastelloy-N were assumed to be constant as shown in Table 3.

Table 3. Properties of FLiBe and Hastelloy-N

Material	ρ (kg/m^3)	c_p (J/kgK)	k (W/mK)	μ (kg/ms)	Pr
Hastelloy-N [14]	8860	578	23.6	-	-
FLiBe [16]	1940	2414.17	1.0	0.0056	13.525

Boundary Conditions

The 2-D computational domain under consideration is depicted in Fig. 2. Louvered fins are characterized as periodic surfaces to reflect their repetitive nature, and a no-slip boundary condition is applied on these surfaces. A constant temperature of 973 K is maintained on the fin walls, considering the melting point of Hastelloy-N lies between 1300–1400°C. The coolant, entering the louvered fins, is kept at 773 K, aligning with the fuel and coolant temperature range of 490–800°C [35]. FLiBe's inlet velocity is set between 0.15–0.80 m/s to ensure laminar flow at the entrance of the louvered fins, and a gauge pressure of 0 Pa is established at the fins' exit. The numerical model's mass, momentum, and energy equations are resolved using Ansys Fluent 14's second-order upwind scheme [36], while the simple algorithm facilitates the efficient coupling of velocity and pressure fields across the coolant's louvered fins [35].

Validation of the Computational Domain

Four different quadrilateral cell sizes were utilized to achieve mesh independence in the 2-D numerical model, as depicted in Fig. 3a. The discrepancies in the solutions for j and f were approximately 0.16% and 0.96%, respectively, for meshes exceeding 90741 nodes. The scarcity of information on FLiBe molten salt flowing over compact heat exchangers with louvered fins presents significant validation challenges for the computational results against literature. The primary difficulty arises not only from the molten salt and compact heat exchanger combination but also from the minimal flow depth in the flat tube used in the CHEX construction.

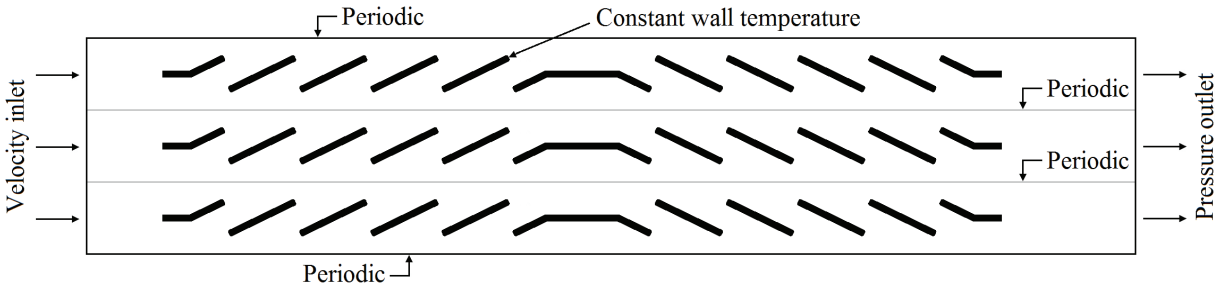

Figure 2. The 2-D numerical model and the boundary conditions.

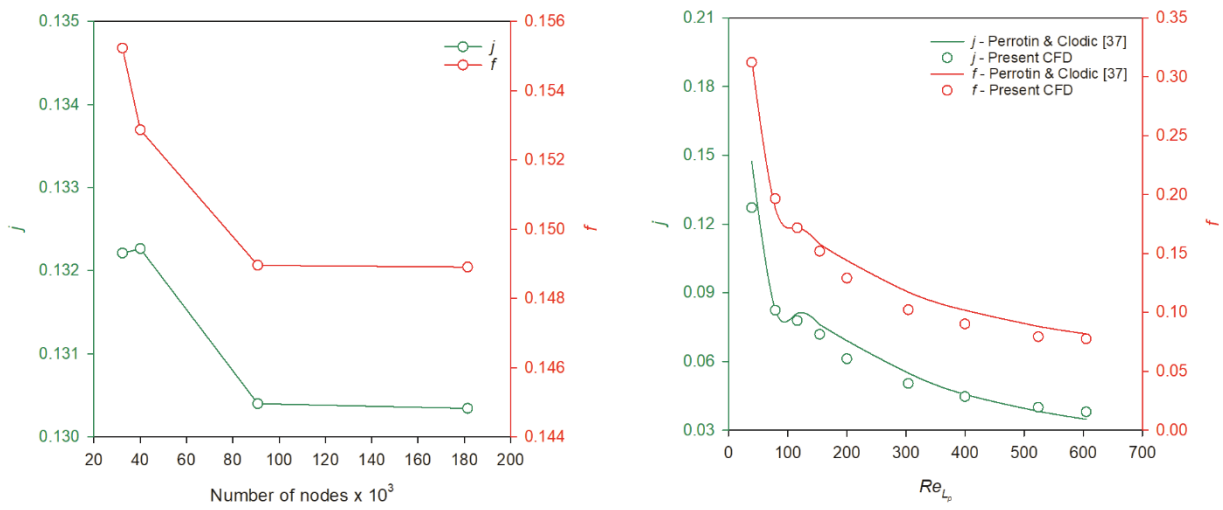

(a) (b)

Figure 3. (a) Mesh independency (b) Comparison of the results with the literature.

In light of these challenges, a fundamental comparison with the numerical study by Perrotin and Clodic is employed for computational model validation. Despite the absence of experimental results on this specific subject, the model's reliability is corroborated by the numerical study's findings. Among the various conditions examined in the study, the configuration with F_p=1.30 mm, L_p=0.95 mm, L_α=20°, F_d=16.5 mm aligns most closely with our current model. There is a notable concordance between the CFD outcomes of present model and the numerical results of Perrotin and Clodic [37].

Mathematical Method

The mathematical model as a result of the numerical approach is presented in this section. The Reynolds number for the coolant side based on the louvered pitch is given as,

$$Re_{Lp} = \frac{u_c L_p}{\upsilon} \tag{9}$$

where

$$u_c = u_{in} \frac{A_{fr}}{A_c} \tag{10}$$

The heat transfer coefficient of the coolant side is determined by using Eq. 11.

$$h = \frac{\dot{Q}}{F A_a \Delta T_m} \tag{11}$$

where the heat transfer rate and logarithmic mean temperature difference are defined as,

$$\dot{Q} = \dot{m} c_p (T_o - T_i) \tag{12}$$

$$\Delta T_m = \frac{T_i - T_o}{ln[(T_s - T_o)/(T_s - T_i)]} \tag{13}$$

In the design of heat exchangers, overall performance criteria are preferred over the direct use of the heat transfer coefficient. The pressure gradient is a crucial design parameter to consider when molten salt flows over louvered fins. The thermal and hydraulic performance of a louvered fin heat exchanger is characterized by the Colburn *j*-factor and the friction factor *f*, as given in Eqs. 14 and 15.

$$j = StPr^{2/3} = \frac{Nu}{Re_{Lp} Pr^{1/3}} \tag{14}$$

$$f = \frac{2\Delta P}{\rho u_c^2} \left(\frac{A_c}{A_a} \right) \tag{15}$$

where

$$St = \frac{h}{\rho u_c C_p} \tag{16}$$

The volume goodness factor of $j/f^{1/3}$ is used for expressing new sights about the overall performance of the louvered fin heat exchanger.

RESULTS AND DISCUSSION

In the present study, the thermo-hydraulic performance of the molten salt FliBe is investigated numerically. The investigation is conducted for varying fluid velocities in the range of 0.1 m/s–0.8 m/s, fin pitches in the range of 1.5–2.5 mm, and fin louver angles in the range of 20°–36°. The findings of the simulations are presented either in dimensional form (heat transfer coefficient vs. frontal velocity, pressure drop vs. frontal velocity) or non-dimensional form (Colburn *j*-factor vs. Re_{Lp} number, *f*-factor vs. Re_{Lp} number). As for the initial step, the contour plots for streamline, pressure, and temperature are demonstrated to provide a better perspective on the flow characteristics of the studied molten salt. Then the thermo-hydraulic performance of the FLiBe is presented by the diagrams that are driven for heat transfer coefficient, pressure drop, Colburn *j*-factor, friction factor *f*, and volume goodness factor $j/f^{1/3}$.

The streamlines which are tangent to the local velocity vectors during the flow of FLiBe are presented in Fig. 4 for the fin pitch F_p=1.5 mm and for the louver angles L_a=20° and 32° where Re_{Lp}=100. These lines are used to observe the inclination of the flow direction during the analyses, as regards to the given figures, when the stream becomes stronger in any direction, the color turns to red from blue. While blue streamlines demonstrate the weaker streams, red corresponds to a stronger flow stream. It could be seen from the schematic, when the louver angle is small (L_a=20°), the molten salt tends to flow through the space between louver fins which causes a lesser interaction between the FLiBe and fin surfaces. On the contrary, the interaction between fin surfaces and FLiBe improves as the louver angle becomes steep. As it is presented in Fig. 4, the streamlines of molten salt flow become stronger, and the color of the streams turns red when FLiBe flows over the fins. It can be noted that, as the louver angle is steeper the flow of the molten salt can be more directed to louver fins and a "louver directed flow" can be obtained vice versa if the louver angle is moderate, molten salt's flow turns to a duct directed flow instead.

The pressure changes along with the louver fins and consequently the drop between the upstream and downstream can be observed from Fig. 5. As it could be seen, as the louver angle turns from L_a=20° to 32°, the pressure changes from upstream to downstream increases. As regards to the presented figure, the pressure of FLiBe is high at the upstream and rises locally in particular at the leading edge in both presented louver angles. The rise at the leading edge is bigger when the fin is steep since the resistance against the flow is higher. As the molten salt flows over the fin, the pressure falls along the flow path and becomes the lowest at the downstream. The pressure difference between the inlet and exit of the molten salt flow is higher when the fin is steeper, and this variance descends as the louver angle becomes more moderate where the resistance against the flow is lower.

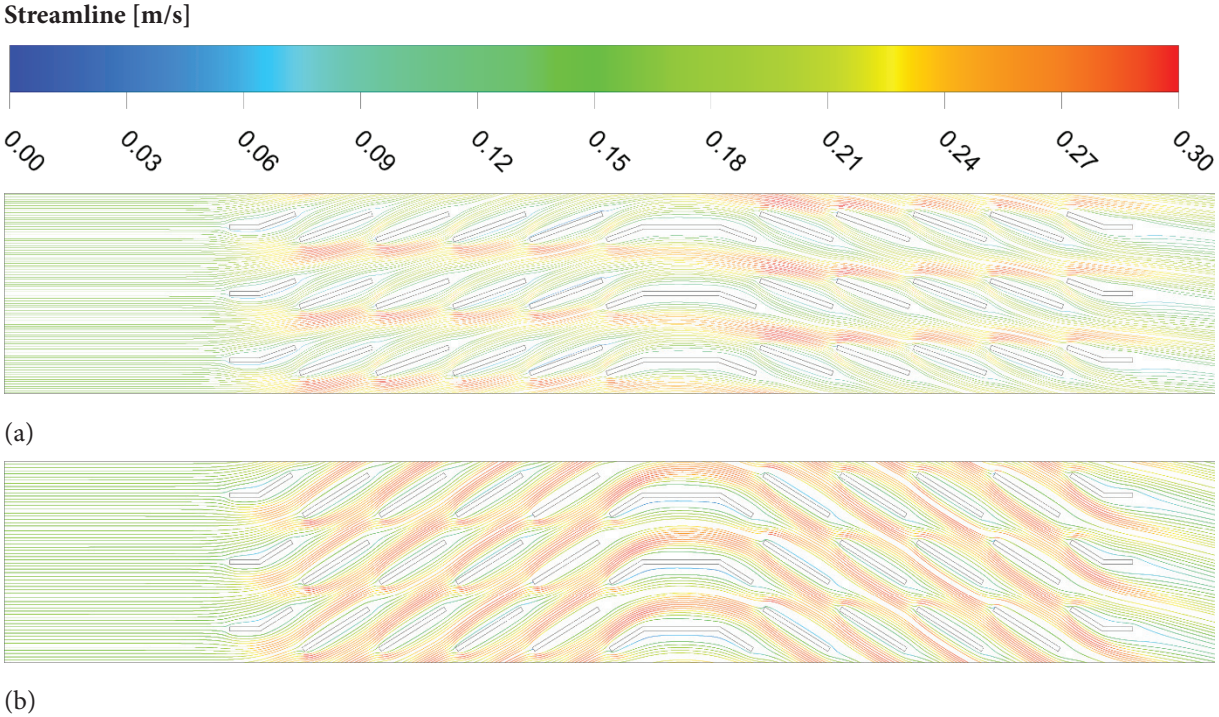

Figure 4. Streamlines of FLiBe flowing through the louvered fins for F_p=1.5 mm and Re_{Lp}=100 (a) L_a=20° (b) L_a=32°.

The temperature distribution along the louver fins is presented in Fig. 6 for the F_p=1.5 mm and L_a=20° and 32° at Re_{Lp}=100. Temperature rises of the molten salt from the upstream to the downstream can be seen clearly in the presented contour plots. While the FLiBe's temperature at the upstream is 773 K at the downstream temperature can rise to 853−873 K locally as regards to heat transfer over the fins to the molten salt. Due to the interaction between the

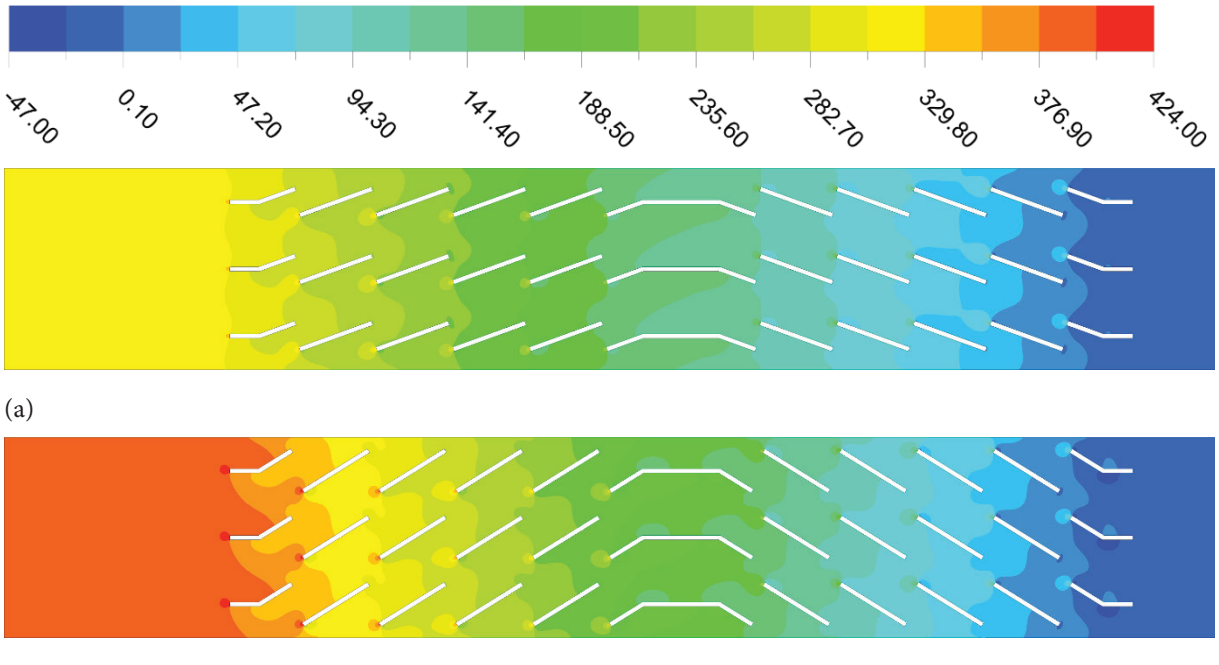

Figure 5. Pressure fields of FLiBe flow through the louvered fins for F_p=1.5 mm and Re_{Lp}=100 (a) L_a=20° (b) L_a=32°.

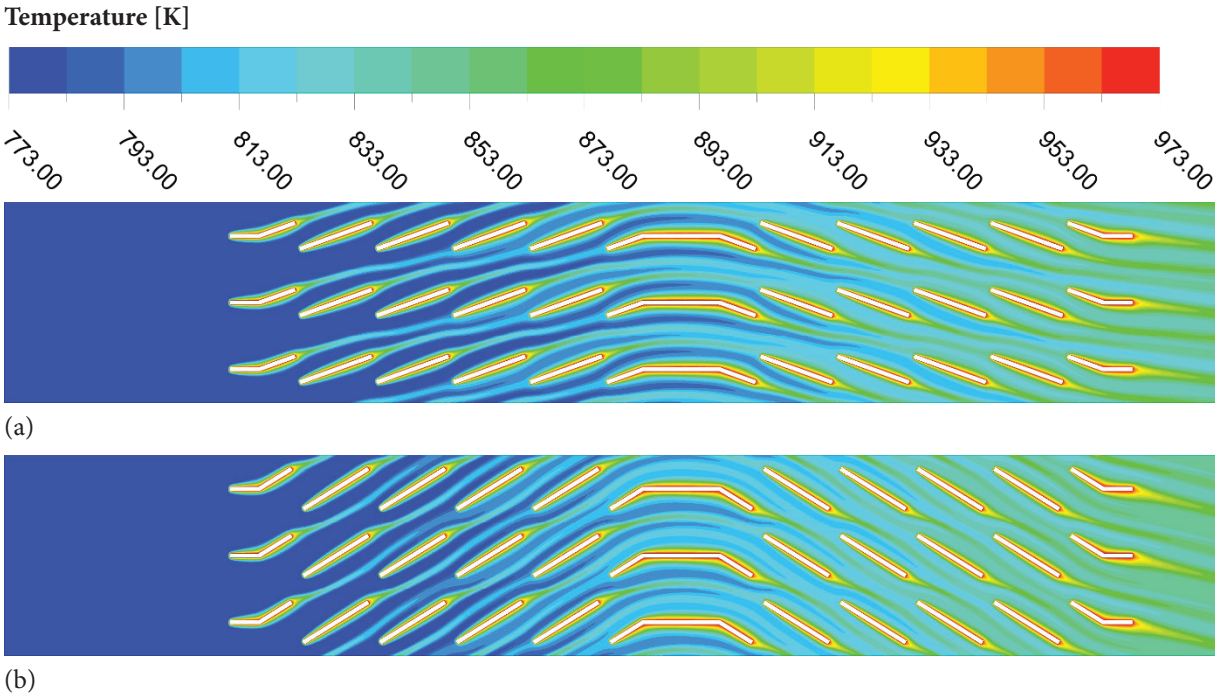

Figure 6. Temperature fields of FLiBe flow through the louvered fins for F_p=1.5 mm and Re_{Lp}=100 (a) L_a=20° (b) L_a=32°.

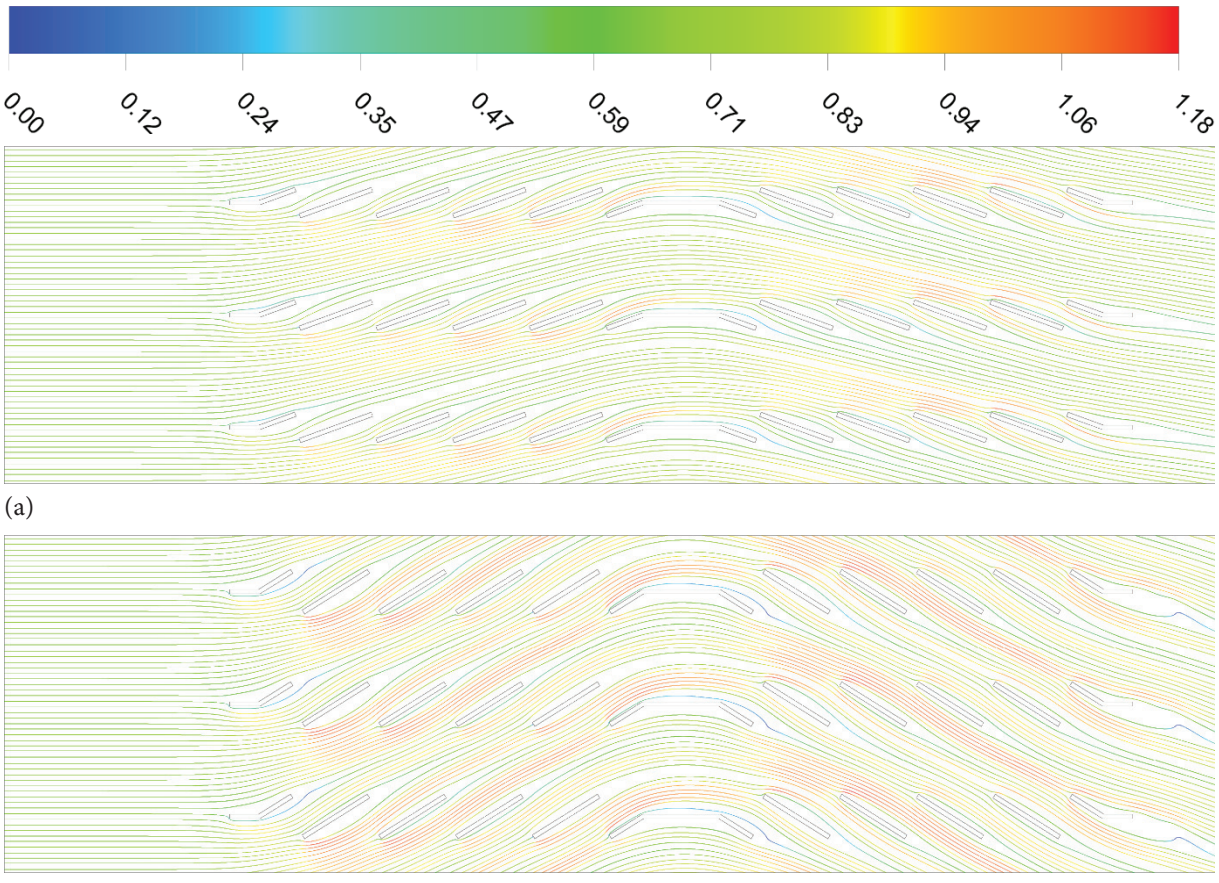

Figure 7. Streamlines of FLiBe flowing through the louvered fins for F_p=2.5 mm and Re_{Lp}=400 a) L_a=20° (b) L_a=32°.

fin surface and FLiBe, more heat is transmitted to the molten salt in the neighboring regions of the fins in which temperature can go up to 950 K as it is plotted in the figures by red color. In accordance with the louver angle increment, the molten salt gains more heat, and the temperature of the molten salt ascends gradually as the L_a rises from 20° to 32°. The temperature of the FLiBe is higher when the louver angle is steep, the major reason for this increment relies on the flow characteristics which are presented in Fig.4. When the louver angle rises, the flow turns from duct directed to louvered directed which improves the interaction between the fins and molten salt, and consequently, the heat transfer is improved.

The evolution of the streamlines, pressure, and temperature by the contour plots are presented for the spacing F_p=2.5 mm in Fig 7-9. To present the findings from a different aspect. A wider fin spacing (F_p=2.5 mm) and higher Reynolds number (Re_{Lp}=400) are chosen in the mentioned figures and temperature, pressure, and streamline contours are plotted for these cases. Once again, the louver angles L_a=20° and 32° are chosen to demonstrate the impact of the louver angle change on the flow characteristics of the molten salt. Similar trends are observed in each figure for the corresponding parameters, such as, while the "duct directed" flow is observed for L_a=20°, it turns to "louvered directed flow" when the louver angle becomes steep (L_a=32°) in Fig 7.

The pressure reduces across the flow direction, the higher pressure is observed at the upstream and lower pressure is seen at the downstream in both louver angles of L_a=20° and 32°. Since the resistance is more when the louver fins are steep, the pressure at the upstream is higher L_a=32° and therefore the pressure difference between inlet and exit is more as it could be seen in Fig. 8.

The temperature distribution over the molten salt increases along the flow direction as well in Fig. 9 during the interaction of the molten salt with fins. Though identical trends are observed, some notable features are detected as well in the demonstrated figures. For instance, even though flow directions are identical, streamlines are sparse due to the higher fin pitch used in this model (Fig. 7). The major reason for this remarkable change is the space

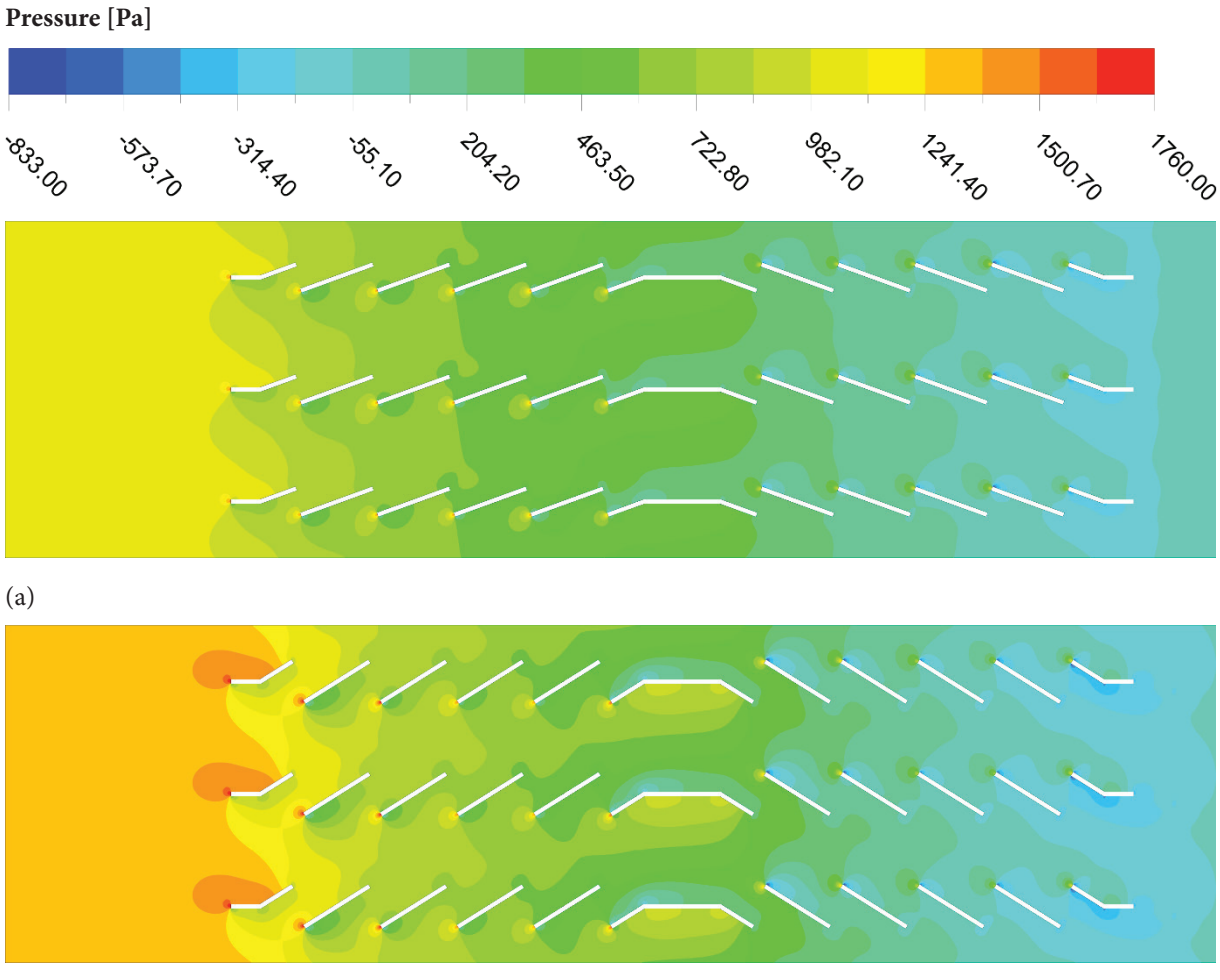

Figure 8. Pressure fields of FLiBe flowing through the louvered fins for F_p=2.5 mm and Re_{Lp}=400 (a) L_a=20° (b) L_a=32°.

between louver fins indicated by the pitch which is F_p=2.5 mm instead. As the space grows, the bigger portion of the molten salt flows through that space instead of flowing over the fins and flow becomes more "duct directed" instead of "louvered directed". This is also the major reason for the worsening thermal performance observed. Fig. 9. As it is seen, the region that gains heat from the fins is very limited since the interaction between the FLiBe and fins gets worse. As the contact reduces and molten salt has more free space to flow, the heat transfer from the fins to the FLiBe gradually descends and the temperature plot has more blue regions which refer to inlet temperature.

Heat transfer coefficient (h) and pressure drop (ΔP), variation with respect to molten salt frontal velocity is presented in Fig.10 for three different fin pitches (F_p=1.5, 2.0, and 2.5 mm). As the velocity increases, the heat transfer performance improves regardless of the variation of the louver angle and fin pitch of the louvered fins. The left-hand side of the figures pertains to heat transfer coefficients, which refers to the curve cluster at the top, while the right-hand side pertains to pressure drop, which refers to the curve cluster at the bottom of the figures. Among the investigated louver angles, the L_a=36° provides the highest heat transfer which gets higher values as the frontal velocity ascends. The major reason for this improvement relies on the flow direction change provided by the variation of the louver angle as presented before with the contour plots. Since the molten salt flow becomes more louver-directed when the louver angle is steep, it enhances the interaction between the FLiBe and fins which leads to a thermal performance increment. The maximum h is obtained as 27000 W/m^{2}K at this louver angle (L_a=36°) and for the velocity of 0.8 m/s among all tested cases, while the lowest is obtained as 12000 W/m^{2}K at (L_a=20°) and for the velocity of 0.1 m/s.

Even though there is a noticeable difference between the louver angle of L_a=36° and the remaining louver angles, this difference is not obvious as the L_a decreases, so h values begin to converge at lower louver angle values and starts to present identical evolution trends by the frontal velocity.

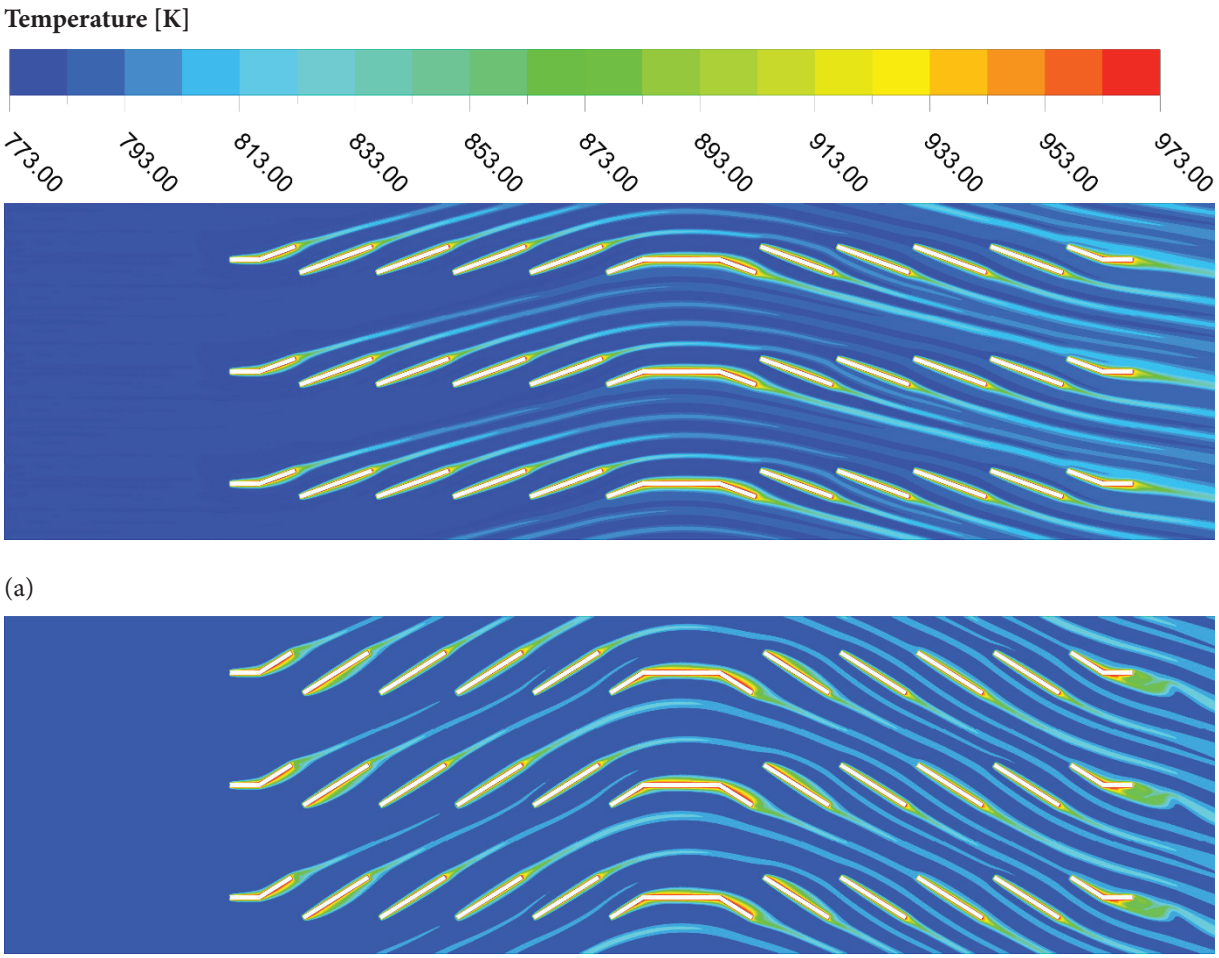

Figure 9. Temperature fields of FLiBe flowing through the louvered fins for F_p=2.5 mm and Re_{Lp}=400 (a) L_a=20° (b) L_a=32°.

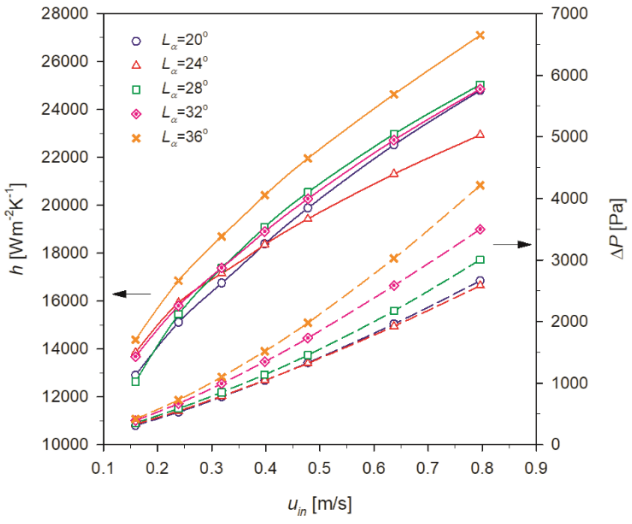

(a)

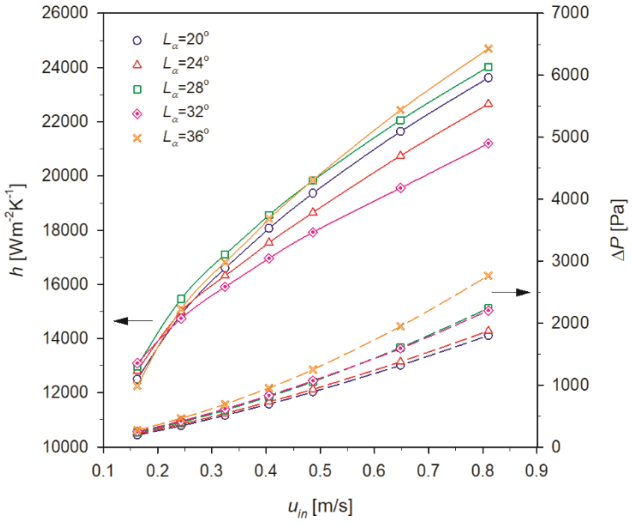

(b)

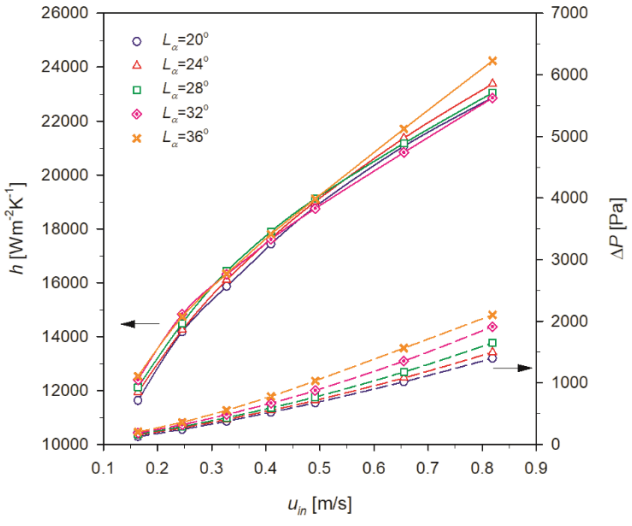

(c)

Figure 10. Deviation of heat transfer coefficient (h) and pressure drop (ΔP) with respect to frontal velocity for FLiBe (u_{in}) (a) F_p=1.5 mm (b) F_p=2.0 mm (c) F_p=2.5 mm.

The evolution characteristics are more obvious for pressure drop (ΔP) curves in the same figure (Fig. 10a). As the louver angle grows, the fins become steep and as a result of increasing pressure at the leading edge, the difference between the upstream and downstream becomes more obvious. The highest pressure drop is obtained for the highest louver angle at the maximum frontal velocity while the lowest is observed for the lowest louver angle and the lowest velocity. The possible reason for the reported change can be related to the louver angle. As the louver angle increases, the resistance against molten salt flow ascends too, which leads to a higher pressure drop. Similarly, as the velocity increases, the pressure drop rises as well. Contradiction to this, as the frontal velocity reduces, pressure drop reduces and when this fall approaches about 0.1 m/s, almost all louver angles show a similar pressure drop across the flow over the fins at this particular velocity. It is seen that the resistance that emerges by the louver angle rise doesn't have an impact at lower frontal velocities as in the higher ones.

Similar evolution trends for heat transfer (h) and pressure drop (ΔP) can be observed for F_p=2.0 mm in Fig. 10b. As it is seen, either h or ΔP increases as the frontal velocity of the molten salt ascends, in addition, both of them rise as the louver angle steeps. Unlike Fig. 10a, h curves of varying louver angles are more obvious at higher frontal velocities. The gradual increment of h plots in each louver angle is clearer than the previous fin pitch. The highest h is obtained around 25000 W/m^{2}K when the L_a=36° and u_{in}=0.8 m/s. As for ΔP, the difference between the plots becomes smaller at this fin pitch but is still apparent. The louver angle changing from L_a=32° to 28° doesn't have much impact on pressure drop and is located between L_a=36° and 24°. Even the L_a=20° has the least ΔP among the analyzed louver angles, ΔP at L_a=24° is very close and there is a vague difference between these two. Fig. 10c demonstrates the heat transfer coefficient (h) and pressure drop (ΔP) evolution for the fin pitch F_p=2.5 mm. Though the trend is identical with the earlier findings, h's are becoming closer than earlier plots which are belonging to fin pitches of 1.5 mm and 2.0 mm. Since the space between the louver fins increases, the duct-directed flow becomes more prominent for the molten salt and as a result, the interaction with the fins descends and thermal performance reduces. Associated with the previous reason, the impact of the louver angle on the thermal performance descends as well and h could be able to reach to 24000 W/m^{2}K, though the ΔP trend and the order among the louver angles are similar, the values of ΔP and curves are plotted on a narrower range, unlike the earlier figures. While pressure drops can go beyond 3000 Pa and be able to reach 4000 Pa for the smaller fin pitches, when the F_p=2.5 mm, the ΔP barley exceeds 2000 Pa.

The Colburn j-factor and friction factor f evolution as regards to Re number for three different fin pitches (F_p=1.5, 2.0, and 2.5 mm) are given in Fig. 11 to see the impact of the louver angle and velocity on the performance from a non-dimensional perspective. The Colburn j-factor and friction

factor *f* reduce as the Re number increases as regards to the nature of these factors' definitions. The highest Colburn *j* -factor is observed for the biggest louver angle in accordance with the earlier findings. The Colburn *j*-factor plots begin to cross over when the louver angle is less than L_a=36° and it seems below this value, louver angle degree does not have much impact on thermo-hydraulic performance when fin pitch is F_p=1.5 mm (Fig 11a). Even though there is a vague difference between the curve for L_a=24° and the rest of them, the variance cannot be reported as a remarkable one. The lowest performance for the Colburn *j*-factor can be marked at this particular condition at around 0.035.

The flow direction which is oriented by the louver angle change has an unavoidable impact on the thermal performance. As the louver angle steeps the flow turns to a louver-directed one and improves the interaction of the fin and molten salt and consequently improves the performance. As for the friction factor *f*, the evolution curves are more observable than the Colburn *j*-factor curves. The overall trend of the friction factor *f* reduces by increasing Re_{Lp} number which can be observed in all investigated louver angles. The highest *f* factor is recorded as 0.52 for the L_a=36° when Re_{Lp} is 100 while the lowest is obtained for L_a=20°–24° when Re_{Lp} is 500. As it is seen, the friction factor at the louver angles L_a=20°–24°, becomes very similar when Re_{Lp} is more than 200. Beyond that threshold, two curves overlap and show identical evolution. As it could be seen, as the louver angle becomes higher, the louver fins position becomes steep against flow which causes higher resistance against the FLiBe flow. Consequently, the pressure drop becomes higher and so the friction factor increases. The exact opposite can be noted too, as the louver angle gets smaller, the flow encounters lower resistance during the flow in particular at lower Reynolds number and it allows smoother transition over the fins. In Fig. 11b, Colburn *j*-factor and friction factor *f* evolution are presented, for F_p=2.0 mm. The overall trend is almost similar with F_p=1.5 mm except for the range that the curves are plotted. While the plots are in the range of 0.10 - 0.04 for F_p=1.5 mm, this range turns to 0.09 to 0.03 for F_p=2.0 mm. The evolution of the Colburn *j*-factor for all louver angles drowns as a cluster for the fin pitch of F_p=2.0 mm. The only observable plot appears for lower louver angles such as L_a=20°. In this particular condition, the lowest performance is observed and plotted below the other investigated louver angles. As for friction factor *f*, the trend is similar to F_p=1.5 mm as well. The highest and lowest plots are pertaining to L_a=36° and 20° respectively. The difference between L_a=20° and 24° at higher Re_{Lp} is more prominent in this case. The highest friction factor *f* is obtained as 0.07 when the L_a=36° and Re_{Lp}=100. The major reason for the highest friction factor for L_a= 36° is the higher resistance that molten salt encounters during the flow which escalates as the louver angle steeps.

Colburn *j*-factor and friction factor *f* change for F_p=2.5 mm is demonstrated in Fig. 11c. Even though they have the same trend, it is becoming hard to distinguish the most

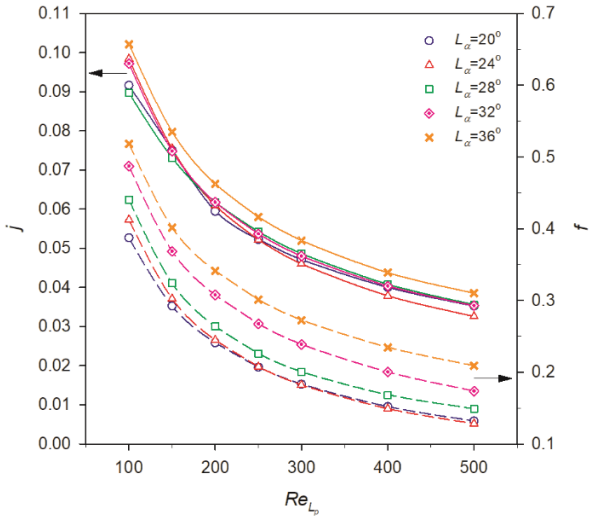

(a)

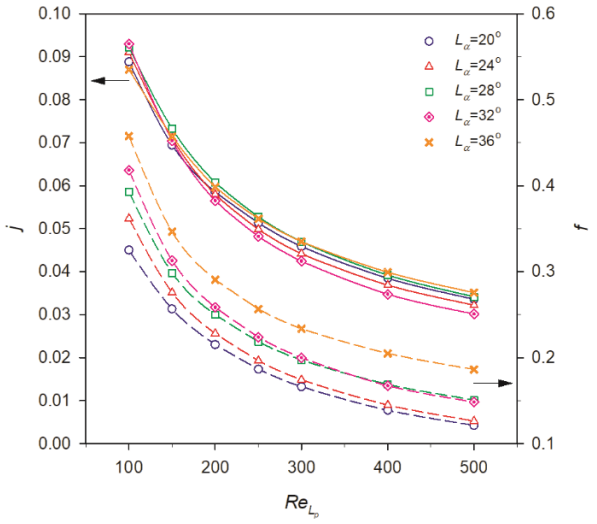

(b)

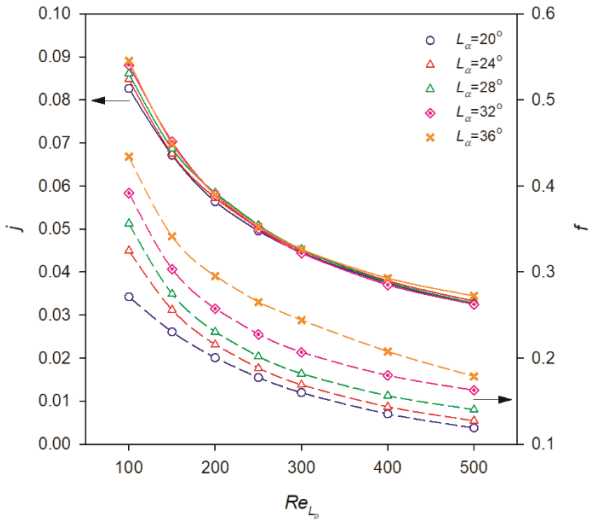

(c)

Figure 11. Deviation of Colburn *j*- and *f*-factors with respect to frontal velocity for FLiBe (a) F_p=1.5 mm (b) F_p=2.0 mm (c) F_p=2.5 mm.

efficient louver angle at this fin pitch since the plot cluster is more congested. The Colburn *j*-factor plots are packed in a narrower range than earlier fin pitches and the impact of the louver angle on the performance becomes very difficult when the space between the fins grows and flow becomes more duct oriented. Unlike Colburn *j*-factor, friction curves are more separated, and the difference between the curves is more obvious as the F_p increases. The highest and lowest friction factors can be identified more clearly. Though the trend has not changed, the maximum friction factor *f* is observed at around 0.43 at the L_a=36° when Re_{Lp} is 100 while the minimum *f* is obtained at around 0.03 at L_a=20° when Re_{Lp} is 500. When the overall picture is considered by taking all diagrams into account, it is seen that all value ranges for *h*, Δ*P*, *j* and *f* reduce as the F_p increases. With regard to summarized findings, thermal performance measures diminish when the fin pitch increases as a consequence of the enlargement of the uninterrupted flow region which refers to the duct-directed flow. As fin pitch becomes lower, the molten salt flow turns to louvered directed flow which enhances the interaction of the fin and FLiBe that allows improving the thermal performance. In addition, the louver angle has an important role in the pressure drop and friction either, as the louver angle steeps, the molten salt encounters more resistance beginning from the leading edge. The trends observed for parameters like the Colburn *j*-factor and *f*-factor are consistent with findings in the literature regarding louver angle and fin pitch [38]. However, differences in magnitude and range arise due to the unique thermophysical properties of molten salt.

The performance of the fins is investigated by some other analogies in literature as well. One of the widely preferred criteria is the volume goodness factor ($j/f^{1/3}$) which allows considering the thermal and hydraulic performance together. The volume goodness factors evolution for all considered louver angles and fin pitches with respect to Re_{Lp} is presented in Fig. 12. In the figures, the findings are presented in three individual schemes which correspond to the fin pitches analyzed in the study. From left to right, the diagrams correspond to the fin pitches of F_p=1.5 mm, 2.0 mm, and 2.5 mm. It could be seen that the overall trend of the volume goodness factor is to descend as the Re_{Lp} increases. Even though every case considered has a similar tendency and obtains values in a similar range which looks like a cluster in each figure, minimum and maximum values are noticeable at each Re_{Lp}. Besides, the unlikely characteristics can be identified among the curve cluster as well. From a wider aspect, for most of the considered Re_{Lp}, the curve pertaining to F_p=2.0 mm and L_a=20° shows better performance while the curve belongs to F_p=2.5 mm and L_a=36° shows the worst performance from the volume goodness factor aspect. The maximum volume goodness factor at Re_{Lp}=100, is obtained as 0.13 and for the case where F_p=1.5 mm and L_a=24° while the lowest value is 0.112 for the louver fins F_p=2.0 mm and L_a=36°. When the Re_{Lp} number is slightly increased there is a minor change in the response of the fins for this increment, unlike the first case, F_p=2.0 mm and L_a=20° shows better performance than other fin pitches and louver angles while F_p=2.5 mm and L_a=36° gets the lowest value. The observed highest and lowest values for this Re_{Lp} are 0.11 and 0.09 respectively. Though the difference isn't very distinct, for the Re_{Lp} number 300 and 400, the highest and lowest performance from the volume goodness aspect, are observed for the louver fins with F_p=2.0 mm and L_a=20° and F_p=2.5 mm and L_a=36°, respectively. Even though the order hasn't changed a lot when Re_{Lp} number is 500, the lowest performance is observed for the louver fin with F_p=2.0 mm and L_a=32° instead. It could be seen; the

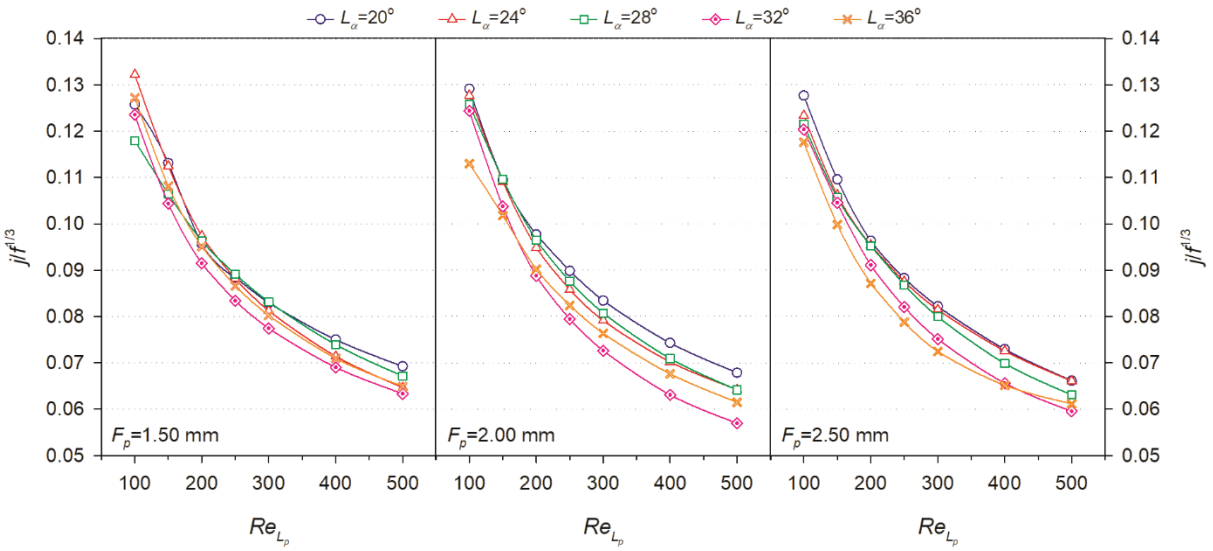

Figure 12. Deviation of volume goodness factor ($j/f^{1/3}$) with respect to Reynolds number.

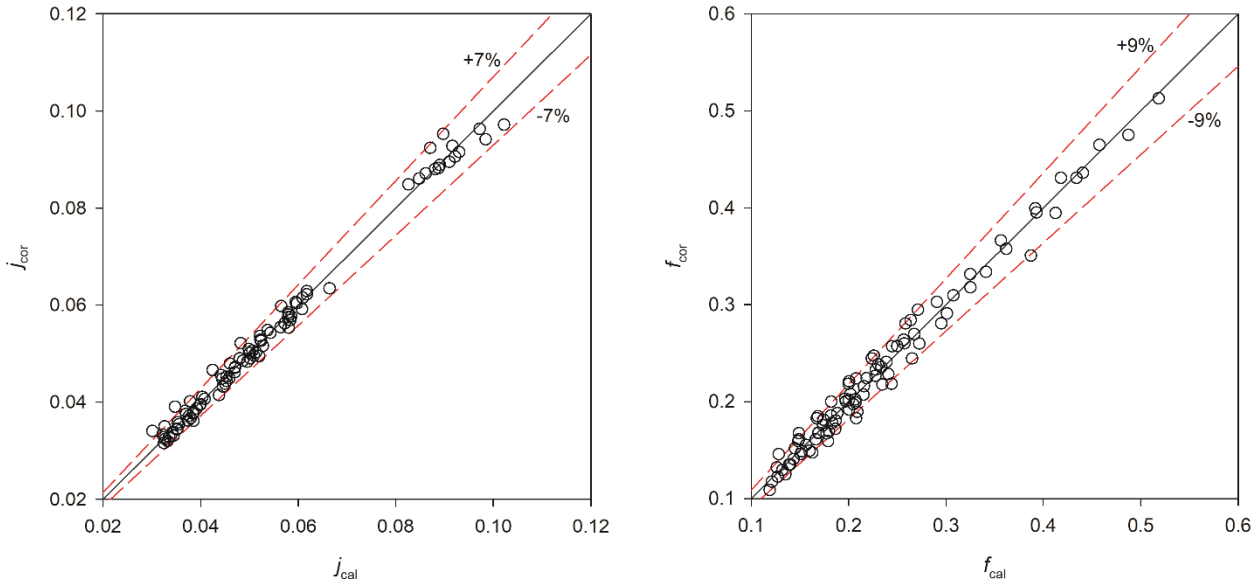

(a) (b)

Figure 13. Comparison of numerical data and correlation for (a) *j*-factor and (b) friction factor.

highest volume goodness factor is obtained as 0.13 while the lowest is observed as 0.06. As regards to outcomes, though the louver fin models with L_a=20° don't show higher performance from both heat transfer and Colburn *j*-factor aspect, when the combined effect of Colburn *j*- and *f*-factors are considered, it becomes the most preferable option among the others since the pressure loss and friction factor values are considerably lower than the other cases.

Finally, the correlations for the Colburn *j*-factor and the friction factor *f* are derived by considering ninety data points, presented in Eqs. 17 and 18, respectively. Fig. 13a and Fig. 13b show the comparison of numerical results with the present correlated data for *j*- and *f*-factors. As can be seen, 95% of the *j*- and *f*-factors data are correlated with in a range of ±7% and ±9%, respectively. The proposed *j*-factor correlation has a mean deviation of 2.55% while the proposed *f*-factor correlation has a mean deviation of 4.55%.

$$j = 1.73(Re_{Lp}^{-0.615})\left(\frac{L_\alpha}{90}\right)^{0.078}\left(\frac{F_p}{L_p}\right)^{-0.175} \quad (17)$$

$$f = 15.36(Re_{Lp}^{-0.619})\left(\frac{L_\alpha}{90}\right)^{0.647}\left(\frac{F_p}{L_p}\right)^{-0.341} \quad (18)$$

CONCLUSION

Minimizing the fuel inventory in the heat exchanger of a molten salt reactor (MSR) is highly desirable. This can be achieved through the use of a compact heat exchanger that maximizes the heat transfer area while minimizing its volume. One of the most promising candidates for such a design is the use of louvered fins over mini-channeled flat tubes. The physical properties of the molten salt in both the primary and secondary fluid circuits influence not only the size and cost of the heat exchanger but also the required pumping power, piping dimensions, fuel inventory, and overall design cost. For the contribution to the molten salt reactor literature, which hasn't been reported before, the steady-state thermo-hydraulic performance of the FLiBe flowing through a compact heat exchanger with multi louvered fins has been investigated with regard to the typical MSR's thermal conditions. A series of numerical tests were conducted for three different fin pitches and five different louver angles in the low-velocity range as part of a preliminary study for an ongoing investigation. Steady-state velocity profiles, temperature distributions, and pressure fields were obtained for five different Reynolds numbers. The heat transfer coefficient and pressure drop were analyzed in terms of the Colburn *j*-factor, the Fanning friction factor *f*, and the volume goodness factor.

The effect of louvered fins, designed to enhance heat transfer, was evaluated. While the heat transfer coefficient improved, it came at the expense of an increased pressure drop. However, the increased pressure drop has a beneficial effect in reducing the fuel inventory. This benchmark study was conducted for low-velocity profiles to assess the suitability of compact heat exchangers for molten salt reactor (MSR) applications. It investigates the thermo-hydraulic behavior of FLiBe as it flows through the louvered fins in a compact heat exchanger (CHX). The outcomes obtained can be highlighted as in the following:

- As the louver angle increases, the upstream pressure rises while the downstream pressure decreases, resulting in a greater overall pressure drop.
- As the louver angle increases, the flow of FLiBe becomes more aligned with the louvers, improving the interaction between the molten salt and the louvered fins, which enhances thermal performance.
- As the fin pitch increases, the flow becomes more duct-directed due to the larger spacing between the fins. This reduces the interaction between the molten salt and the fins, leading to a decline in the thermal performance of the compact heat exchanger (CHX).
- As the velocity of the molten salt flow increases, both the heat transfer coefficient and the pressure drop rises for all investigated fin pitches and louver angles. The highest heat transfer coefficient range is obtained for F_p=1.5 mm by 12000-28000 W/m^{2}K, while this range changes as 12000-25000 W/m^{2}K and 12000-24000 W/m^{2}K for the F_p=2.0 mm and F_p=2.5 mm respectively. A similar decrement is observed when the fin pitch impact is observed on the pressure drop. The ΔP range is 4500-0 Pa for F_p=1.5 mm, while it reduces to 3000-0 Pa and 2000-0 Pa for F_p=2.0 mm and F_p=2.5 mm respectively.
- The Colburn *j*-factor and *f*-factor decrease as the Reynolds number increases, regardless of the fin pitch or louver angle. As the fin pitch increases, thermal performance declines due to reduced interaction, resulting in a corresponding decrease in the Colburn *j*-factor range. While it evolves in the range of 0.10–0.04 for the F_p=1.5 mm, it drops to 0.095–0.03 and 0.09–0.03 for the F_p=2.0 mm and F_p=2.5 mm respectively. The same trend is observed for the friction factor too.

This study bridges two key fields: MSRs and the design of compact heat exchangers with enhanced heat transfer surface areas. As such, it provides valuable insights for researchers, product designers, and manufacturers working on the thermohydraulic systems of MSRs. As highlighted by the summarized findings, this comprehensive investigation into the thermohydraulic of FLiBe under boundary conditions relevant to MSRs contributes to the development of more efficient compact heat exchangers. These advancements enhance heat transfer from the reactor core, enabling reduced system volume and minimizing the fuel salt inventory outside the core.

NOMENCLATURE

A_a	air side heat transfer area, m^2
A_c	minimum flow area, m^2
A_{fr}	frontal area, m^2
c_p	specific heat at constant pressure, J·kg^{-1}·K^{-1}
f	friction factor
F	correction factor
F_d	flow depth, mm
F_h	fin height, mm
F_p	fin pitch, mm
h	heat transfer coefficient, W·m^{-2}·K^{-1}
j	Colburn j-factor
k	thermal conductivity, W·m^{-1}·K^{-1}
L_α	louver angle, °
L_h	louver height, mm
L_p	louver pitch, mm
$\dot{m}$	mass flow rate, kg·s^{-1}
P	pressure, Pa
Pr	Prandtl number
$\dot{Q}$	heat transfer rate, W
Re_{Lp}	Reynolds number based on louver pitch
St	Stanton number
t	thickness of the louvered fin, mm
T	temperature, K
T_i	inlet temperature, K
T_d	tube depth, mm
T_p	tube pitch, mm
T_o	outlet temperature, K
T_s	surface temperature, K
ΔT_m	logarithmic mean temperature difference, K
V	velocity, m·s^{-1}
u_c	maximum velocity at minimum flow area, m·s^{-1}
u_{in}	free flow velocity at the inlet, m·s^{-1}

Greek letters

α	thermal diffusivity, m^2·s^{-1}
μ	dynamic viscosity, kg·m^{-1}·s^{-1}
ρ	density, kg·m^{-3}
υ	kinematic viscosity, m^2·s^{-1}

Abbreviations

ANP	Aircraft Nuclear Propulsion
ARE	Aircraft Reactor Experiment
FOM	Figure of Merit
MSBR	Molten Salt Breeder Reactor
MSRE	Molten Salt Reactor Experiment
MSRs	Molten Salt Reactors
NGNP	Next Generation Nuclear Plant
ORNL	Oak Ridge National Laboratory
TEMA	Tubular Exchanger Manufacturers Association
THORIMS-NES	Thorium Molten Salt Nuclear Energy Synergetic

REFERENCES

[1] Guo Z, Zhou J, Zhang D, Chaudri KS, Tian W, Su G, et al. Coupled neutronics/thermal-hydraulics for analysis of molten salt reactor. Nucl Eng Des 2013;258:144–156. [CrossRef]

[2] Furukawa K, Mitachi K, Kato Y, Chigrinov SE, Lecocq A, Erbay LB, et al. Rational Pu-disposition for U-production by THORIMS-NES (thorium molten-salt nuclear energy synergetics). Presented at: IAEA Meeting; 1995; Vienna, Austria. p. 169–181.

[3] Furukawa K, Arakawa K, Erbay LB, Ito Y, Kato Y, Kiyavitskaya H, et al. A road map for the realization of global-scale thorium breeding fuel cycle by single molten-fluoride flow. Energy Convers Manag 2008;49:1832–1848. [CrossRef]

[4] Furukawa K, DE Greaves, Berrin Erbay L, Hron M, Kato Y. New sustainable secure nuclear industry based on thorium molten-salt nuclear energy synergetics (THORIMS-NES). In: Tsvetkov P, (editor). Nuclear Power – Deployment, Operation and Sustainability. London: IntechOpen; 2011. [CrossRef]

[5] Furukawa K, Berrin Erbay L, Aykol A. A study on a symbiotic thorium breeding fuel-cycle: THORIMS-NES through FUJI. Energy Convers Manag 2012;63:51–54. [CrossRef]

[6] MacPherson RE. Gas cooled molten salt heat exchanger. Oak Ridge (TN): Oak Ridge National Laboratory; 1958.

[7] Alexander LG, Kinyon BW, Lackey ME, MacPherson RE, Miller JW, VanderLage FC, et al. Experimental molten salt fuelled 30 MW power reactor. Oak Ridge (TN): Oak Ridge National Laboratory; 1960.

[8] Robertson RC. MSRE design and operations report part I: description and reactor report. Oak Ridge (TN): Oak Ridge National Laboratory; 1965.

[9] Cantor S. Density and viscosity of several molten fluoride mixtures. Oak Ridge (TN): Oak Ridge National Laboratory; 1973.

[10] Erbay LB. Examining the power generation by the Stirling heat engine combined with the molten salt reactor. In: ECOS'99; 1999; Tokyo, Japan. p. 429–434.

[11] Akram W, Parvez M, Khan O. Parametric analysis of solar-assisted trigeneration system based on energy and exergy analyses. J Therm Eng 2023;9:764–775. [CrossRef]

[12] Erbay LB. Knowhow of Th-MSR heat exchange system. Presented at: 11th International Conference on Sustainable Energy Technologies; 2012; Vancouver, Canada.

[13] Lippy MS. Development of a minichannel compact primary heat exchanger for a molten salt reactor [dissertation]. Blacksburg (VA): Virginia Polytechnic Institute and State University; 2011. [CrossRef]

[14] Valerio A. Heat exchanger analysis for innovative molten salt fast reactor [master thesis]. Villigen (Switzerland): Paul Scherrer Institute; 2014.

[15] Kloosterman JL, Köse U, Koç U, Erbay LB, Öğüt E, Ayhan H, et al. Heat exchanger design studies for molten salt fast reactor. EPJ Nucl Sci Technol 2019;5:12. [CrossRef]

[16] Manohar SS, Matthias AE, Piyush S, Phil S. Engineering database of liquid salt thermophysical and thermochemical properties. Idaho Falls (ID): Idaho National Laboratory, U.S. DOE Nuclear Energy Office; 2010.

[17] Tufeu R, Petitet JP, Denielou L, Le Neindre B. Experimental determination of the thermal conductivity of molten pure salts and salt mixtures. Int J Thermophys 1985;6:315–330. [CrossRef]

[18] Sahin S. Selection criteria for fusion reactor structures. J Therm Eng 2019;5:46–57. [CrossRef]

[19] Bin L, Yu-ting W, Chong-fang M, Meng Y, Hang G. Turbulent convective heat transfer with molten salt in a circular pipe. Int Commun Heat Mass Transf 2009;36:912–916. [CrossRef]

[20] Wu Y-T, Chen C, Liu B, Ma C-F. Investigation on forced convective heat transfer of molten salts in circular tubes. Int Commun Heat Mass Transf 2012;39:1550–1555. [CrossRef]

[21] Lu J, He S, Ding J, Yang J, Liang J. Convective heat transfer of high temperature molten salt in a vertical annular duct with cooled wall. Appl Therm Eng 2014;73:1519–1524. [CrossRef]

[22] He S, Lu J, Ding J, Yu T, Yuan Y. Convective heat transfer of molten salt outside the tube bundle of heat exchanger. Exp Therm Fluid Sci 2014;59:9–14. [CrossRef]

[23] He S, Ding J, Lu J, Wang W, Yang J. The heat transfer characteristics of molten salts flowing in a vertical concentric duct. Energy Proced 2014;61:2629–2632. [CrossRef]

[24] Ferng YM, Lin K-Y, Chi C-W. CFD investigating thermal-hydraulic characteristics of FLiNaK salt as a heat exchange fluid. Appl Therm Eng 2012;37:235–240. [CrossRef]

[25] Srivastava AK, Vaidya AM, Maheshwari NK, Vijayan PK. Heat transfer and pressure drop characteristics of molten fluoride salt in circular pipe. Appl Therm Eng 2013;61:198–205. [CrossRef]

[26] Rodríguez-Sánchez MR, Marugan-Cruz C, Acosta-Iborra A, Santana D. Comparison of simplified heat transfer models and CFD simulations for molten salt external receiver. Appl Therm Eng 2014;73:993–1005. [CrossRef]

[27] Carasik LB, Shaver DR, Haefner JB, Hassan YA. Steady RANS methodology for calculating pressure drop in an in-line molten salt compact crossflow heat exchanger. Prog Nucl Energy 2017;101:209–223. [CrossRef]

[28] Colliva F, Hattab F, Siriano S, Ferrero G, Meschini S, Testoni R, et al. Conceptual design and supporting analysis of a double wall heat exchanger for an ARC-class fusion reactor primary cooling system. Fusion Eng Des 2024;201:114261. [CrossRef]

[29] Du B-C, He Y-L, Qiu Y, Liang Q, Zhou Y-P. Investigation on heat transfer characteristics of molten salt in a shell-and-tube heat exchanger. Int Commun Heat Mass Transf 2018;96:61–68. [CrossRef]

[30] He Y-L, Zheng Z-J, Du B-C, Wang K, Qiu Y. Experimental investigation on turbulent heat transfer characteristics of molten salt in a shell-and-tube heat exchanger. Appl Therm Eng 2016;108:1206–1213. [CrossRef]

[31] Sabharwall P, Clark D, Glazoff M, Zheng G, Sridharan K, Anderson M. Advanced heat exchanger development for molten salts. Nucl Eng Des 2014;280:42–56. [CrossRef]

[32] Parker Hannifin. What is a Heatric printed circuit heat exchanger? Available at: https://ph.parker.com/us/en/product-list/heatric-printed-circuit-heat-exchanger. Accessed on Dec 1, 2024.

[33] Kim ES, Sabarwall P, Anderson N. Development of figure of merits (FOMs) for intermediate coolant characterization and selection. Presented at: American Nuclear Society Annual Meeting; 2011; Hollywood, Florida.

[34] Chang Y-J, Wang C-C. A generalized heat transfer correlation for louver fin geometry. Int J Heat Mass Transf 1997;40:533–544. [CrossRef]

[35] Brovchenko M, Heuer D, Merle-Lucotte E, Allibert M, Capellan N, Ghetta V, et al. Preliminary safety calculations to improve the design of molten salt fast reactor. Presented at: Advances in Reactor Physics – Linking Research, Industry, and Education; 2012; Knoxville, Tennessee. p. 1–12.

[36] ANSYS Inc. ANSYS Fluent user's guide. Release 14.0. Canonsburg (PA): ANSYS Inc.; 2011.

[37] Perrotin T, Clodic D. Thermal-hydraulic CFD study in louvered fin-and-flat-tube heat exchangers. Int J Refrig 2004;27:422–432.

[38] Kim M-H, Bullard CW. Air-side thermal hydraulic performance of multi-louvered fin aluminum heat exchangers. Int J Refrig 2002;25:390–400.